

Vesicle-Specific Noble Gas Analyses of "Popping Rock": Implications for Primordial Noble Gases in Earth

Pete Burnard,* David Graham, Grenville Turner

Gases trapped in individual vesicles in the volatile-rich basaltic glass "popping rock" were found to have the same carbon dioxide, helium-4, and argon-40 composition, but a variable $^{40}\text{Ar}/^{36}\text{Ar}$ ratio (~ 4000 to $\geq 40,000$). The argon-36 is probably surface-adsorbed atmospheric argon; any mantle argon-36 trapped in the vesicles cannot be distinguished from an atmospheric contaminant. Consequently the $^{40}\text{Ar}/^{36}\text{Ar}$ ratios and $^3\text{He}/^{36}\text{Ar}$ ratios (1.45) determined are minimum estimates of the upper mantle composition. Heavy noble gas relative abundances in the mantle resemble solar noble gas abundance patterns, and a solar origin may be common to all primordial mantle noble gases.

The noble gases (He, Ne, Ar, Kr, and Xe) are important for tracing the volatile history of Earth because they are not recycled back to the mantle during subduction [with the possible exception of Xe (1)] and several radiochronometers are recorded in the isotopic compositions of He, Ne, Ar, and Xe. Nonradiogenic noble gases that were trapped during accretion of Earth are still present in the mantle and are outgassing at mid-ocean ridge crests and ocean islands (2). The relative proportions of radiogenic and primordial noble gas isotopes are dependent on the extent and timing of episodes of gas loss from the mantle. Several mantle degassing models have been proposed to account for the noble gas isotopic compositions of the atmosphere and mantle reservoirs (1, 3–8). From analyses of noble gases in oceanic basalts, we examined the likely starting material for these degassing models, that is, the noble gas inventory trapped during accretion of Earth.

The isotopic composition of He and Ne trapped in mantle-derived rocks distinguishes two mantle regions: the well-mixed mid-ocean ridge basalt (MORB) source region with a near constant $^4\text{He}/^3\text{He}$ ratio of $\sim 90,000$ (equivalent to a $^3\text{He}/^4\text{He}$ ratio of $8R_a$, where R_a is the atmospheric $^3\text{He}/^4\text{He}$ ratio of 1.39×10^{-6}), and a reservoir sampled by some ocean island basalts (OIBs) with lower $^4\text{He}/^3\text{He}$ ratios than MORBs [the lowest recorded values of $\sim 20,000$ (equivalent to a $^3\text{He}/^4\text{He}$ ratio of $35R_a$) are from the Loihi Seamount (9)]. Because ^{21}Ne in the mantle is mostly produced by (α, n) reaction on ^{18}O , production of ^{21}Ne

and production of ^4He are both related to U+Th concentrations (10, 11). The volatiles trapped in OIBs are also characterized by less radiogenic (lower) $^{21}\text{Ne}/^{22}\text{Ne}$ ratios than those trapped in MORBs, consistent with higher time-integrated (U+Th)/ ^3He and (U+Th)/ ^{22}Ne ratios in the MORB source region. Mantle degassing models (steady-state upper mantle models) have been postulated in which all primordial noble gases reside in the lower mantle (equated with the OIB source region) and are transferred into the upper mantle (MORB source region) by plumes (1, 3, 5, 6). The higher $^4\text{He}/^3\text{He}$ and $^{21}\text{Ne}/^{22}\text{Ne}$ ratios of MORBs are due to the accumulation of radiogenic ^4He and ^{21}Ne during residence in the upper mantle for ~ 1 billion years (3, 5, 6).

In contrast to He and Ne, the heavy noble gas (Ar, Kr, and Xe) isotopic compositions of MORBs and OIBs are difficult to distinguish. For Ar, this is because of the high abundance of relatively nonradiogenic Ar in the atmosphere ($^{40}\text{Ar}/^{36}\text{Ar} = 295.5$) coupled with highly radiogenic Ar in mantle samples [$^{40}\text{Ar}/^{36}\text{Ar} \geq 12,000$ for OIBs (12) and $\geq 28,000$ in MORBs (13, 14)]. It has not been possible to distinguish ^{36}Ar derived from the mantle from atmospheric contaminants, and all $^{40}\text{Ar}/^{36}\text{Ar}$ analyses of mantle samples are lower limits to the value of the mantle source region. It is also not possible to assert conclusively that the lower $^{40}\text{Ar}/^{36}\text{Ar}$ ratios analyzed in some OIBs compared with some MORBs are due to lower $^{40}\text{Ar}/^{36}\text{Ar}$ ratios in the OIB mantle source region. The equivalent problems do not arise for the light noble gases because atmospheric contamination is less significant due to physico-chemical differences and their lower abundances in the atmosphere. Furthermore, because there are three isotopes of Ne, the three end-members (atmosphere, MORB, and OIB source regions) can be deconvolved.

There are few samples of OIB glass that have erupted at the sea-water depths required to prevent extensive volatile loss from the erupting magma. In a steady-state upper mantle, however, nonradiogenic noble gas isotope ratios, such as $^3\text{He}/^{36}\text{Ar}$, will be the same in the upper and lower mantle. It may be possible, therefore, to deduce the lower mantle nonradiogenic isotope compositions of noble gases by analyzing volatile-rich MORB glasses. The most volatile-rich basaltic glass analyzed to date is the "popping rock" ($2\pi\text{D43}$) with up to 17% vesicularity, which was dredged off the mid-Atlantic ridge in 1985. This extraordinary sample has been analyzed several times (13, 15–17); the current $^{40}\text{Ar}/^{36}\text{Ar}$ value (28,000) for the upper mantle is based on analyses of popping rock, as are estimates of the carbon content of the MORB source region. Noble gas elemental abundances are consistent with minimal gas loss or fractionation during transport from mantle to surface (13, 17).

Using laser extraction techniques (18), we reanalyzed the popping rock. Laser extraction, as well as having low and consistent ^{36}Ar blank levels (18), also allows ^{36}Ar adhering to the sample surface to be assessed. We show here that all the ^{36}Ar released from this sample may have been adhering to the surface and that the $^{40}\text{Ar}/^{36}\text{Ar}$ ratio of the upper mantle is significantly higher than previously thought ($\geq 40,000$).

The $^{40}\text{Ar}/^{36}\text{Ar}$ ratios in popping rock vesicles ranged from ~ 4000 to $\sim 40,000$ (Table 1). One analysis produced a value of 64,000, but we are reluctant to adopt this value as a MORB lower limit. This single analysis is clearly separate from the majority of results, and the high $^{40}\text{Ar}/^{36}\text{Ar}$ ratio arises from an abnormally low ^{36}Ar release rather than a high ^{40}Ar release, unlike the other high $^{40}\text{Ar}/^{36}\text{Ar}$ analyses (Table 1). The $^{40}\text{Ar}/^{36}\text{Ar}$ ratios are correlated with $\text{CO}_2/^{36}\text{Ar}$ (Fig. 1) and $^4\text{He}/^{36}\text{Ar}$ ratios. These results are consistent with addition of a variable atmospheric contaminant having high ^{36}Ar abundances to a low- ^{36}Ar mantle fluid with a uniform $\text{CO}_2\text{-}^4\text{He-}^{40}\text{Ar}^*$ composition (where $^{40}\text{Ar}^*$ is ^{40}Ar corrected for atmospheric Ar). The $\text{CO}_2\text{-}^4\text{He-}^{40}\text{Ar}^*$ compositions (Table 1) are constant (within error) for all the vesicles we analyzed ($\text{CO}_2/^4\text{He} = 3.69 \pm 0.24 \times 10^4$ and $^4\text{He}/^{40}\text{Ar}^* = 0.99 \pm 0.03$). The amount of ^{36}Ar released by laser-gas-rich vesicles is indistinguishable from that released by laser-gas-free regions of glass (Fig. 2), which typically have an $^{40}\text{Ar}/^{36}\text{Ar}$ ratio closer to that of atmospheric Ar (~ 300 ; Fig. 2). Atmospheric Ar, either adhering to the surface of the sample section or dissolved within the glass structure, can account for all the ^{36}Ar detected. Mantle

P. Burnard and G. Turner, Department of Earth Sciences, University of Manchester, Manchester M13 9PL, UK.

D. Graham, College of Oceanic and Atmospheric Sciences, Oregon State University, Corvallis, OR 97331, USA.

*To whom correspondence should be addressed. E-mail: peteb@man.ac.uk

³⁶Ar trapped in the vesicles of popping rock could not be detected.

The range in ⁴⁰Ar/³⁶Ar ratios reported here is due primarily to a large range in the amount of ⁴⁰Ar released, because the amount of ³⁶Ar released is more constant (Fig. 2). Similar systematics are likely to control ⁴⁰Ar/³⁶Ar ratios determined by conventional noble gas techniques (crushing or step-heating). The highest ⁴⁰Ar/³⁶Ar analyses reported in the literature are from samples with high volatile contents such as popping rock. Glasses from ocean islands have very low volatile abundances; for example, the highest ⁴⁰Ar* concentrations in submarine glasses from the Loihi Seamount are two orders of magnitude lower than in popping rock. It is plausible that low ⁴⁰Ar/³⁶Ar ratios measured in OIB glasses are due to low ⁴⁰Ar abundances in the samples, while the adhered atmospheric contaminant remains relatively constant.

A magma ascending beneath a mid-ocean ridge will decompress until C solubility is exceeded and CO₂ bubbles form. At this point, the noble gases dissolved in the magma will partition between the vapor and melt depending on their solubilities (19). As noble gas solubilities decrease with increasing mass (and atomic size) in basaltic melts (20), the He/Ar ratio in the vapor will be lower than in the melt. Noble gas solubilities are well known and obey Henry's law, making it possible to predict the rate of He/Ar fractionation in both vapor and melt during magma degassing. Furthermore, as He and Ar in the upper mantle are dominated by their radiogenic isotopes, it is possible to predict He/Ar (\cong ⁴He/⁴⁰Ar*), in the source region using comparatively well constrained mantle K/(U+Th) composi-

tions; He and Ar are both extremely incompatible (20), and consequently the He/Ar ratio in the parent magma will be the same as in the source region. With a K/U ratio of 12,700 (21) and a Th/U ratio of 2.6 (22), the upper mantle accumulated radiogenic ⁴He/⁴⁰Ar* ratio is likely to be between 2 and 3 (depending on the accumulation time and the proportion of He and Ar transferred from lower to upper mantle). Because ³He/³⁶Ar fractionates at the same rate as ⁴He/⁴⁰Ar, it is simple to correct ³He/³⁶Ar ratios for fractionation by multiplying by [⁴He/⁴⁰Ar]_{initial}/⁴He/⁴⁰Ar]_{measured}. The unfractionated ³He/³⁶Ar ratio for popping rock estimated by this method is \geq 1.45 using a ⁴He/³He ratio of 88,000 (13, 16, 17) because ³He was not measured directly in this study.

Previous (bulk sample) analyses of the ⁴He/⁴⁰Ar* ratio in popping rock range from 1.2 to 2.8 (13, 16), higher than the ratio we measured (0.99 \pm 0.03). Although there appear to be heterogeneities in the volatile composition trapped in various pieces of this sample, the major element glass composition of this piece, determined by electron microprobe, is similar to the glass composition of other pieces of popping rock (17). The volatiles trapped in this piece are consistent with gas exsolved from a previously unfractionated magma such that \sim 50% of the total He remained in the magma. This is also compatible with computed Rayleigh fractionation trajectories in the He-Ar-CO₂ system. The higher ⁴He/⁴⁰Ar* ratios in other pieces of popping rock may result from more complete magmatic degassing such that all the He and Ar was present in the gas phase. The piece analyzed here is less vesicular (\sim 5%) than some

pieces of popping rock (up to 17%), indicating a difference in volatile history between the various pieces of popping rock. The He/Ar ratios and vesicle contents in this piece are broadly consistent with a lower proportion of the gases having exsolved from the magma.

A direct implication of the steady-state upper mantle models is that the primordial noble gas isotope ratios in the upper and lower mantle are the same, whereas the ⁴⁰Ar/³⁶Ar ratios in each mantle region are related by the fraction of Ar transferred from

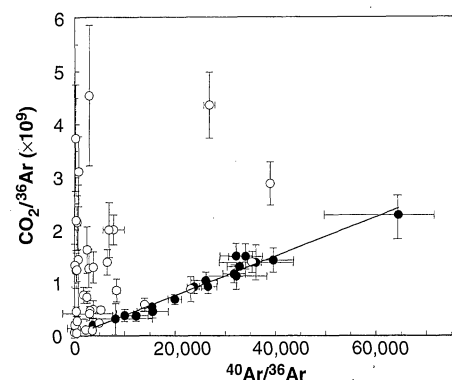


Fig. 1. Correlation between CO₂ and ⁴⁰Ar in popping rock vesicles. Open symbols, glass only; closed symbols, vesicles. Mixing between a mantle-derived end-member having a constant CO₂/⁴⁰Ar of 37,200 (given by the slope of the line shown) and a variable, atmosphere-derived ³⁶Ar-rich component explains the observed trend. The uncontaminated mantle-derived component must have an ⁴⁰Ar/³⁶Ar ratio equal to or greater than the highest values obtained here.

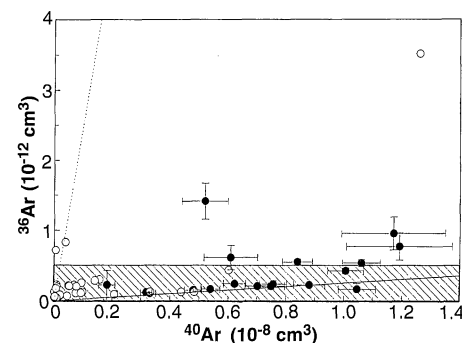


Fig. 2. The ⁴⁰Ar and ³⁶Ar released by individual laser shots into popping rock. Symbols as in Fig. 1. Lines with a slope corresponding to atmospheric Ar (dashed line, ⁴⁰Ar/³⁶Ar = 296) and the lower limit of the mantle component (solid line, ⁴⁰Ar/³⁶Ar = 40,000) are plotted for reference. Some of the high ⁴⁰Ar "glass only" analyses (open symbols) are likely to have ⁴⁰Ar accidentally released from adjacent or not visible vesicles. There is no difference in the amount of ³⁶Ar released when laserling vesicle-free regions of the sample (indicated by the shaded area) or when laserling open a vesicle. All the ³⁶Ar analyzed (even in the highest ⁴⁰Ar/³⁶Ar analyses) may have been released from the surface of the sample.

Table 1. Results from laser extraction of individual vesicles in popping rock (2πD43). Analyses are all blank corrected in cubic centimeters at standard temperature and pressure (STP). Vesicles that were empty (because of decrepitation during sample preparation or clean-up procedures) are not presented in the table but are included for comparison in Figs. 1 and 2.

Analysis	⁴ He (x10 ⁻⁹)	⁴⁰ Ar (x10 ⁻⁹)	CO ₂ (x10 ⁻⁵)	⁴⁰ Ar/ ³⁶ Ar
2/1a3	13.0 ± 0.5	11.7 ± 1.8	35 ± 4	12,000 ± 2,000
2/1a13	5.6 ± 0.2	5.2 ± 0.8	27 ± 3	3,600 ± 400
2/1a4	6.1 ± 0.2	6.1 ± 0.9	23 ± 2	10,000 ± 2,000
2/1a5	1.9 ± 0.1	1.8 ± 0.3	7 ± 1	8,000 ± 7,000
2/1a6	12.3 ± 0.5	11.9 ± 1.8	34 ± 4	15,000 ± 3,000
3/1a13	8.0 ± 0.7	7.6 ± 0.5	26 ± 3	32,000 ± 6,000
3/1a17	7.2 ± 0.6	7.5 ± 0.5	29 ± 3	36,000 ± 7,000
3/1a3	10.2 ± 0.9	10.6 ± 0.7	36 ± 4	20,000 ± 1,000
3/1a4	6.5 ± 0.6	6.2 ± 0.4	25 ± 3	26,000 ± 2,000
3/1a7	8.9 ± 0.8	8.8 ± 0.5	32 ± 3	40,000 ± 4,000
3/1a8	7.2 ± 0.6	7.0 ± 0.4	31 ± 3	34,000 ± 3,000
3/1a9	4.7 ± 0.4	4.8 ± 0.3	22 ± 2	32,000 ± 3,000
4/1a12	5.8 ± 0.5	5.4 ± 0.3	21 ± 2	33,000 ± 2,000
4/1a14	10.2 ± 0.9	10.5 ± 0.6	37 ± 4	64,000 ± 8,000 (-15,000)
4/1a2	8.9 ± 0.8	8.4 ± 0.5	29 ± 3	15,400 ± 600
4/1a7	10.5 ± 0.9	10.1 ± 0.6	39 ± 4	24,000 ± 1,000
4/1a8	3.7 ± 0.3	3.2 ± 0.2	11 ± 1	27,000 ± 2,000
4/1a9	3.9 ± 0.3	3.3 ± 0.2	12 ± 1	32,000 ± 2,000

the lower mantle to the upper mantle (5, 6). In the Porcelli and Wasserburg model (6), the lower mantle $^{40}\text{Ar}/^{36}\text{Ar}$ ratio is about one-third of the ratio of the upper mantle. Therefore, the Ar isotopic composition of MORBs can be used to constrain the minimum $^{40}\text{Ar}/^{36}\text{Ar}$ ratio of the lower mantle. Using the Porcelli and Wasserburg steady-state upper mantle model, we estimate that the minimum possible $^{40}\text{Ar}/^{36}\text{Ar}$ ratio of the lower mantle is $\sim 14,000$. Assuming a steady-state upper mantle, the minimum lower mantle $^3\text{He}/^{36}\text{Ar}$ ratio is 1.45.

It has not been possible to distinguish the nonradiogenic isotopes of Ar, Kr, and Xe in mantle material from those in the atmosphere [with the possible exception of Xe in Harding County well gas (23)]. The nonradiogenic isotopes of Ar, Kr, and Xe present in oceanic basalts may be dominated by atmospheric noble gases (24–26) from surface contamination, as seen in this study, or from recycling of atmospheric noble gases trapped in subducted sediments to the mantle (1).

Noble gases in the solar system can be broadly subdivided into planetary, as found in chondrites and the atmospheres of Earth, Mars, and Venus, and solar, as produced in solar flares and implanted into orbiting bodies such as meteorites and the moon. Solar noble gases are enriched in light elements such as He and Ne relative to Ar and Xe, and in light isotopes. Estimates of the relative abundances of the nonradiogenic Ar and Xe in the mantle are upper limits because of the uncertainties in the extent of atmospheric contamination. Nevertheless, the mantle abundances of nonradiogenic Ar and Xe relative to He and Ne are less than for the planetary noble gas component (Fig. 3). Unless extreme fractionation has occurred, nonplanetary heavy noble gases are present in the mantle.

It has been established that solarlike Ne is present in the mantle (27). If atmospheric noble gases were derived from mantle outgassing, extreme fractionation of Ne isotopes must have occurred to account for the atmospheric Ne isotopic composition (28). An alternative scenario is that mantle Ne is solar and atmospheric Ne is largely planetary and did not originate from mantle outgassing (7, 11). As we have demonstrated, there is no evidence for planetary noble gases in the mantle, and this scenario can be extended to all the mantle noble gases. Therefore, all nonradiogenic mantle noble gases may be solar in origin.

If the nonradiogenic noble gases in the mantle are solar, then the mantle contribution to atmospheric noble gases must be small; a separate origin for the atmosphere is implied, such as a late, volatile-rich accretionary veneer (29). However, some mantle-derived gases are present in the atmosphere. Atmospheric ^{40}Ar is likely to be from the mantle (^{40}Ar cannot be primordial), and atmospheric He (which has a short residence time in the atmosphere because of gravitational escape) is from present-day mantle outgassing. Also, the atmospheric $^{20}\text{Ne}/^{22}\text{Ne}$ ratio (9.8) is slightly higher than the planetary Ne composition (~ 8.5); addition of some solar Ne ($^{20}\text{Ne}/^{22}\text{Ne} \sim 13.5$), which may be from mantle degassing, to the atmosphere can account for the difference (7).

These minimum estimates of the mantle $^3\text{He}/^{36}\text{Ar}$ ratio tend toward the solar value of 12.6 to 15 (30) and are three orders of magnitude greater than the planetary $^3\text{He}/^{36}\text{Ar}$ ratio of <0.001 (31). If the primordial noble gas relative abundances in the mantle are solar in composition, it would be difficult to distinguish nonradiogenic Ar, Kr, or Xe from atmospheric contaminants. For instance, if we assume an unfractionated solar

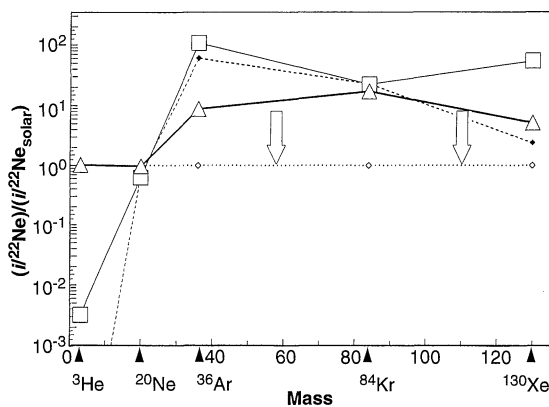
$^3\text{He}/^{36}\text{Ar}$ ratio in the lower mantle of 12, then lower mantle $^{40}\text{Ar}/^{36}\text{Ar}$ ratios of 135,000 (32) and upper mantle values in excess of 400,000 are predicted.

The existence of solar Ar in the mantle could be confirmed by measuring $^{38}\text{Ar}/^{36}\text{Ar}$ ratios lower than the atmospheric value ($^{38}\text{Ar}/^{36}\text{Ar}_{\text{Solar}} = 0.182$; $^{38}\text{Ar}/^{36}\text{Ar}_{\text{Atmosphere}} = 0.188$) in oceanic basalts. This is an exceptionally difficult ratio to measure because of the large ^{40}Ar signal present when performing the analysis. Furthermore, the rough calculation above demonstrates that current extraction techniques are not likely to detect solar Ar in the mantle: the ^{36}Ar and ^{38}Ar from an unfractionated solarlike mantle source will be completely swamped by atmospheric contaminants unless we can reduce current levels of contamination by an order of magnitude.

Two-stage Earth accretion models (33) (where planetary Ar, Kr, and Xe are accreted after solar He and Ne) may be unnecessarily complicated because there is no direct evidence for planetary noble gases in the mantle. It is likely that the accreting planetesimals that formed Earth were mostly degassed of their planetary noble gases as a result of the extreme energies involved in accretion (34); the naked, degassed protoplanet that formed would then inherit solar-pattern noble gases during orbit around the sun. Mantle-atmosphere and Earth evolution models that are sensitive to mantle $^{40}\text{Ar}/^{36}\text{Ar}$ composition require reevaluation in the light of the data presented here. For example, estimation of lower mantle–upper mantle mass fluxes with growth models of the mantle $^{40}\text{Ar}/^{36}\text{Ar}$ ratio (35) are likely to overestimate the mass flux. Furthermore, these models cannot define a precise mass flux but can only limit the maximum amount of mass transfer, because it is not yet possible to precisely define $^{40}\text{Ar}/^{36}\text{Ar}$ in either mantle reservoir.

Direct analyses of popping rock provide lower limits for the upper mantle $^{40}\text{Ar}/^{36}\text{Ar}$ and $^3\text{He}/^{36}\text{Ar}$ ratios of $\geq 40,000$ and ≥ 1.45 , respectively; application of steady-state upper mantle models to these data imply that the lower mantle $^{40}\text{Ar}/^{36}\text{Ar}$ and $^3\text{He}/^{36}\text{Ar}$ ratios are $\geq 14,000$ and ≥ 1.45 , respectively. The emerging mantle noble gas abundance patterns show greater similarity to solar abundances than to planetary abundances, and there is no isotopic evidence requiring planetary noble gases in the mantle. Mantle Ne is certainly solar in composition, and it now seems reasonable to extend a solar origin to all mantle noble gases.

Fig. 3. The abundances of noble gases normalized to Ne, relative to solar compositions. Open diamonds, solar; filled diamonds, atmosphere; open squares, planetary; open triangles, mantle; and *i* refers to the isotope on the x axis. Mantle ^{36}Ar compositions were calculated assuming a steady-state upper mantle and with mass fluxes (6): $[\text{Ar}]_{\text{lm}} = [\text{Ar}]_{\text{um}} - [\text{Ar}]_{\text{atm}} \approx [\text{Ar}]_{\text{um}} \times 0.33 \leq 5.7 \times 10^{14} / (40,000 \times 0.33) \leq 4.1 \times 10^{10}$ atoms g^{-1} . Lm denotes lower mantle; um denotes upper mantle. $[\text{Ar}]_{\text{lm}}$, the lower mantle ^{40}Ar production, is calculated from estimates of mantle ^{40}K abundances in (6). All mantle compositions



are calculated for no recycling of noble gases (to represent initial compositions). Mantle $^{130}\text{Xe}/^{22}\text{Ne}$ and $^{84}\text{Kr}/^{22}\text{Ne}$ ratios are from previous analyses of popping rock (13). It is important to note that the heavy noble gas (Ar, Kr, Xe) relative abundances are all maximum estimates, as indicated by the arrows. Solar and planetary data from (30, 31); atmospheric abundances from (28).

REFERENCES AND NOTES

1. D. Porcelli and G. Wasserburg, *Geochim. Cosmochim. Acta* **59**, 1991 (1995).
2. J. Lupton and H. Craig, *Earth Planet. Sci. Lett.* **26**,

- 133 (1975); B. A. Mamyrin, I. N. Tolstikhin, G. S. Anufriev, I. L. Kamanskiy, *Dokl. Akad. Nauk SSSR* **184**, 1197 (1969); W. B. Clarke, M. A. Beg, H. Craig, *Earth Planet. Sci. Lett.* **6**, 213 (1969).
3. L. H. Kellogg and G. J. Wasserburg, *Earth Planet. Sci. Lett.* **99**, 276 (1990).
4. C. J. Allègre, T. Staudacher, P. Sarda, *ibid.* **81**, 127 (1986).
5. R. K. O'Nions and I. N. Tolstikhin, *ibid.* **124**, 131 (1994).
6. D. Porcelli and G. J. Wasserburg, *Geochim. Cosmochim. Acta* **59**, 4921 (1995).
7. B. Marty, *Earth Planet. Sci. Lett.* **94**, 45 (1989).
8. _____ and P. Allègre, in *Noble Gas Geochemistry and Cosmochemistry*, J. Matsuda, Ed. (Terra Scientific, Tokyo, 1994), pp. 191–204.
9. M. D. Kurz, W. J. Jenkins, S. R. Hart, D. Clague, *Earth Planet. Sci. Lett.* **66**, 388 (1983).
10. G. W. Wetherill, *Phys. Rev.* **96**, 679 (1954).
11. M. Honda, I. McDougall, D. Patterson, A. Dougeris, D. Clague, *Nature* **349**, 149 (1991); P. Sarda, T. Staudacher, C. J. Allègre, *Earth Planet. Sci. Lett.* **91**, 73 (1988).
12. R. Poreda and K. Farley, *Earth Planet. Sci. Lett.* **113**, 129 (1992).
13. T. Staudacher *et al.*, *ibid.* **96**, 119 (1989).
14. D. E. Fisher, *ibid.* **123**, 199 (1994).
15. F. Pineau and M. Javoy, *ibid.*, p. 179.
16. M. Javoy and F. Pineau, *ibid.* **107**, 598 (1991).
17. P. H. Sarda and D. Graham, *ibid.* **97**, 268 (1990); D. Graham and P. Sarda, *ibid.* **105**, 568 (1991).
18. The analytical technique used is slightly modified from (25). Thick sections (~300 μm) were thoroughly cleaned and loaded into an ultra high-vacuum chamber with glass viewports. Selected vesicles were lasered with short (<0.5 s) pulses using a continuous wave (CW) yttrium-aluminum-garnet-Nd (YAG Nd) laser (~3 W power; beam diameter < 100 μm). The pressure increase resulting from gas released from the vesicles was measured by capacitance manometer (MKS Baratron) within a calibrated volume (0.2 liter). A small sample (~5%) was abstracted and analyzed for major gas (CO_2 , H_2O , N_2 , and CH_4) composition. The remaining gas was purified (using two SAES NP10 getters) and separated into He and Ar fractions with liquid N_2 -cooled activated charcoal, and these fractions were subsequently analyzed with a VG5400 noble gas mass spectrometer. Procedural blanks were continually monitored (on average, three blanks were performed per analysis) and maintained at very low and consistent levels by careful vacuum practice. The total variation in ^{36}Ar blank (2σ) during the 6-week analysis period was $1.5 \times 10^{-13} \text{ cm}^3 \text{ STP}$ with variations on a day-to-day basis of $0.8 \times 10^{-13} \text{ cm}^3 \text{ STP}$; typical blank levels were $< 6 \times 10^{-13} \text{ cm}^3 \text{ STP}$. All ^{36}Ar analyses presented here are 2σ or more above the blank, not lower limits calculated with the system detection capabilities. ^{40}Ar and ^4He blanks do not affect the data (<1% of a typical sample).
19. M. Y. Spasnykh and I. N. Tolstikhin, *Geochem. J.* **27**, 213 (1993).
20. M. R. Carroll and E. M. Stolper, *Geochim. Cosmochim. Acta* **57**, 5039 (1993).
21. K. P. Jochum, A. W. Hofmann, E. Ito, H. M. Seufert, W. M. White, *Nature* **306**, 431 (1983).
22. R. K. O'Nions and D. McKenzie, *Philos. Trans. R. Soc. London Ser. A* **342**, 65 (1995).
23. D. Phinney, J. Tennyson, U. Frick, *J. Geophys. Res.* **83**, 2313 (1978).
24. K. A. Farley and H. Craig, *Geochim. Cosmochim. Acta* **58**, 2509 (1994).
25. P. G. Burnard, F. M. Stuart, G. Turner, *Earth Planet. Sci. Lett.* **128**, 243 (1994).
26. D. B. Patterson, M. Honda, I. McDougall, *Geophys. Res. Lett.* **17**, 705 (1990).
27. Radiogenic and nucleogenic production of ^{20}Ne and ^{22}Ne within the mantle is negligible, therefore the mantle $^{20}\text{Ne}/^{22}\text{Ne}$ ratio is related to the primordial (that is, trapped during accretion) Ne isotope composition. Mantle samples have $^{20}\text{Ne}/^{22}\text{Ne}$ ratios up to ~13 (1), distinct from the atmospheric value of 9.8. Solar $^{20}\text{Ne}/^{22}\text{Ne}$ ratios are between 13.3 and 13.8 (30), consistent with solar Ne trapped in the mantle.
28. D. M. Hunten, R. O. Pepin, J. C. B. Walker, *Icarus* **69**, 532 (1987).
29. T. Owen, A. Bar-Nun, I. Kleinfeld, *Nature* **358**, 43 (1992).
30. A. Pedroni and F. Begeman, *Meteoritics* **29**, 632 (1994); J.-P. Benkert, H. Baur, P. Signer, R. Wieler, *J. Geophys. Res.* **98**, 13 (1993); R. Wieler and H. Baur, *Meteoritics* **29**, 570 (1992); R. H. Becker and R. O. Pepin, *Earth Planet. Sci. Lett.* **103**, 55 (1991); R. Wieler, H. Baur, P. Signer, *Geochim. Cosmochim. Acta* **50**, 1997 (1986).
31. T. Swindle, in *Meteorites and the Early Solar System*, J. F. Kerridge and M. S. Matthews, Eds. (Univ. of Arizona Press, Tucson, 1988), pp. 535–564.
32. The calculated production of ^{40}Ar and ^4He in the lower mantle (lm) is 5.7 and $10 \times 10^{14} \text{ atoms g}^{-1}$, respectively (6). Assuming $^4\text{He}/^3\text{He}_{\text{lm}} = 20,000$, then $^3\text{He}_{\text{lm}} = 10 \times 10^{14}/20,000 = 5 \times 10^{10} \text{ atoms g}^{-1}$. If the mantle trapped solar He and Ar relative abundances, then $^3\text{He}/^{36}\text{Ar}_{\text{lm}} = 12$ to 15, $^{36}\text{Ar}_{\text{lm}} = [^3\text{He}]_{\text{lm}}/12 = 4.2 \times 10^9$ to $3.3 \times 10^9 \text{ atoms g}^{-1}$ and $^{40}\text{Ar}/^{36}\text{Ar} = 135,000$ to 171,000.
33. C. L. Harper Jr. and S. B. Jacobsen, *Science* **273**, 1814 (1996).
34. G. W. Wetherill, *ibid.* **228**, 877 (1985); H. J. Melosh, *Impact Cratering: A Geologic Process*, vol. 11 of *Oxford Monographs on Geology and Geophysics*, H. Charnock *et al.*, Eds. (Oxford Univ. Press, Oxford, 1989).
35. R. K. O'Nions and I. N. Tolstikhin, *Earth Planet. Sci. Lett.* **139**, 213 (1996).
36. Supported by the Natural Environment Research Council BRIDGE initiative (grant GST/02/1139). Thanks to T. Glenn for technical wizardry. The manuscript was considerably improved by the comments of two anonymous reviewers.

16 December 1996; accepted 20 February 1997

Climatic Limits on Landscape Development in the Northwestern Himalaya

Nicholas Brozović,*† Douglas W. Burbank, Andrew J. Meigs‡

The interaction between tectonism and erosion produces rugged landscapes in actively deforming regions. In the northwestern Himalaya, the form of the landscape was found to be largely independent of exhumation rates, but regional trends in mean and modal elevations, hypsometry (frequency distribution of altitude), and slope distributions were correlated with the extent of glaciation. These observations imply that in mountain belts that intersect the snowline, glacial and periglacial processes place an upper limit on altitude, relief, and the development of topography irrespective of the rate of tectonic processes operating.

On scales of years to thousands of years, mountains are generally viewed as approximately static masses of rock whose surfaces are etched by erosion (1). In contrast, on scales of tens of thousands to millions of years, tectonic and geomorphic processes may lead to the exhumation of rocks once buried tens of kilometers in the crust (2). Typically the presence of elevated topography has been interpreted as a response to enhanced rates of rock uplift, whereas apparent altitudinal limits to topography have been interpreted in terms of rock strength or gravitational collapse (3–5). Here, we compared indices of exhumation and geomorphic and climatic data with digital topographic analysis and found that in the actively deforming northwestern Himalaya, climate is the fundamental control on the development of topography.

Our study area covered more than 40,000 km^2 of the northwestern Himalaya and Karakoram (Fig. 1). The juxtaposition

of deeply incised river gorges and mountain peaks forms the world's largest, steepest terrestrial relief: in less than 30 km the elevation drops from 8125 and 7788 m at the summits of Nanga Parbat and Rakaposhi, respectively, to about 1500 m in the Indus and Hunza valleys. This relief creates an altitudinal zonation of climatic, ecologic, and geomorphic regimes (6, 7). Much of the landscape is dominated by glacial and periglacial processes, and a southwest-to-northeast gradient of decreasing annual precipitation controls the lower altitudinal limit of permanent snow (the snowline) and the extent of glaciation (6–8). Sediment yield, bedrock incision, and historic landslide data (9, 10) indicate that modern-day erosion rates are uncommonly high (up to 12 mm/year along the middle Indus gorge).

On the basis of relief and degree of dissection, we divided our study area into eight distinct physiographic regions consisting of undissected plateaus, dissected plateaus, and deeply incised mountainous regions (Fig. 2A). Each region has an area of several thousand square kilometers, and the boundaries between regions were taken either at the mid-points of major valleys or along major faults or structural trends. We used a 90-m grid space digital elevation model

Department of Earth Sciences, University of Southern California, Los Angeles, CA 90089, USA.

*Present address: Department of Geology and Geophysics, University of California, Berkeley, CA 94720, USA. E-mail: nick@moray.berkeley.edu

†To whom correspondence should be addressed.

‡Present address: Division of Geological and Planetary Sciences, California Institute of Technology, Pasadena, CA 91125, USA.